Marine Chemistry 267 (2024) 104453

Contents lists available at ScienceDirect

Marine Chemistry

journal homepage: www.elsevier.com/locate/marchem

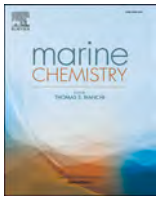

A comparative study of optical and size properties of dissolved organic matter in the lower Mississippi River and Pearl River

Zhengzhen Zhou [a,b], Hui Lin [a,c], Eurico J. D'Sa [d], Laodong Guo [a,b,*]

[a] School of Freshwater Sciences, University of Wisconsin-Milwaukee, 600 East Greenfield Avenue, Milwaukee, WI 53204, USA
[b] Department of Marine Science, University of Southern Mississippi, 1020 Balch Blvd., Stennis Space Center, MS 39529, USA
[c] Polar Research Institute of China, 1000 Xuelong Rd, Pudong, Shanghai 201209, China
[d] Department of Oceanography and Coastal Sciences, Louisiana State University, Baton Rouge, LA 70803, USA

ARTICLE INFO

Keywords:
Dissolved organic matter
CDOM
Fluorescence EEM
Colloidal organic carbon
Mississippi River
Pear River

ABSTRACT

Monthly water samples were collected from the lower Mississippi and Pearl Rivers between January 2009 and August 2011 to investigate the heterogeneity in the dynamic variations of dissolved organic carbon (DOC), colloidal organic carbon, chromophoric and fluorescence dissolved organic matter (CDOM and FDOM), PARAFAC-derived fluorescent components, and other optical properties including spectral slope, specific UV absorbance (SUVA), and fluorescence indices between the two contrasting river systems. The lower Mississippi River exhibits relatively lower concentrations of DOC (306 ± 41 μM C) and CDOM (27.9 ± 5.7 m^{-1} at 254 nm), featuring lower aromaticity (indicated by $SUVA_{254}$) and apparent molecular weight (or higher spectral slope) with weak seasonal variability. The Pearl River, in contrast, has elevated levels of DOC (537 ± 212 μM C) and CDOM (66.4 ± 31.4 m^{-1}), characterized by higher aromaticity, higher molecular weight, and significant seasonality, primarily originating from soil-derived allochthonous sources. The abundance of the >1 kDa colloidal DOC was, on average, 58 ± 3 % of the bulk DOC in the lower Mississippi River and 68 ± 6 % in the lower Pearl River. The >1 kDa high-molecular weight DOM (HMW-DOM) consistently had lower spectral slope and biological index (BIX) values, but higher humification index (HIX) values compared to both bulk DOM and low-molecular-weight DOM (LMW-DOM) counterparts. These trends could be representative of other similar large and small rivers. Four PARAFAC-derived fluorescent components (three humic-like and one protein-like) were identified for both rivers. A positive correlation between discharge and terrestrial humic-like fluorescent components indicated their dominant allochthonous sources, while the protein-like component decreased with increasing discharge, consistent with its autochthonic source and a dilution effect during high flow seasons. The occurrence of large flood events during the sampling period contributed to large DOC pulses, with DOM of higher aromaticity and HMW-DOM. This has important implications for coastal ocean ecosystems, which are increasingly impacted by river flooding events under changing climate conditions. Our results also provide an improved understanding of DOM dynamics in two representative rivers and establish a baseline dataset for future studies to assess changes in sources and composition of DOM and their impacts on the coastal ocean in response to climate, hydrological, and anthropogenic influences.

1. Introduction

Globally, dissolved organic carbon (DOC) export from rivers to the ocean is approximately 0.25 Gt annually (Aitkenhead and McDowell, 2000), with the top 30 largest rivers in terms of discharge contributing over 51 % of the total global flux (Raymond and Spencer, 2015). Riverine dissolved organic matter (DOM) has been found to influence estuarine and coastal marine ecosystems (Bianchi et al., 1997; Findlay et al., 1998; Joung et al., 2019) and is thus a major component in marine carbon cycles (Bianchi, 2013; Hedges et al., 1997). Knowledge of composition and sources of DOM and their temporal variability in river systems is important for a better understanding of the transport and fate of riverine DOM delivered to the oceans, and the biogeochemical processes at the land-ocean interface, especially influenced by large rivers such as the Mississippi River (D'Sa and DiMarco, 2009; Duan et al., 2013; Fichot and Benner, 2014; Cai et al., 2015; Raymond and Spencer,

* Corresponding author at: School of Freshwater Sciences, University of Wisconsin-Milwaukee, 600 East Greenfield Avenue, Milwaukee, WI 53204, USA.
E-mail address: guol@uwm.edu (L. Guo).

https://doi.org/10.1016/j.marchem.2024.104453
Received 1 March 2024; Received in revised form 22 August 2024; Accepted 13 September 2024
Available online 14 September 2024

2015). Further, extreme climate and weather events such as extreme precipitation in river basins increasingly driven by climate change are likely to influence the export fluxes of DOM quantity and quality and the biogeochemical processes in the coastal ocean (Bauer et al., 2013; Hounshell et al., 2019; Lu and Liu, 2019; D'Sa et al., 2023; Liu et al., 2023).

Natural DOM is ubiquitous in aquatic environments and has been shown to be highly heterogeneous along the aquatic continuum (Aiken et al., 2011; Xu and Guo, 2017; Lin et al., 2023). The abundance and composition of riverine DOM, as well as its diagenetic state, chemical/biological reactivity and ultimate fate, are largely controlled by its source material, land use, extent of in situ riverine processes, and other hydrological and biogeochemical processes in rivers and their drainage basins (Duan et al., 2007a; Findlay and Sinsabaugh, 1999; Guo et al., 2012; Lu et al., 2013; Xu et al., 2018; Lin et al., 2021). The diverse sources and high molecular complexity of DOM make it difficult to capture variations in riverine DOM characteristics based on discretionary sampling, especially in large rivers such as the Mississippi River (Duan et al., 2007a) and time series sampling is needed (Jaffé et al., 2008; Cai et al., 2015; Lin et al., 2021).

Chromophoric (CDOM) and fluorescent (FDOM) dissolved organic matter represent important DOM fractions often used to characterize DOM composition (Coble, 1996; Helms et al., 2008). Indeed, optical signatures of absorption and fluorescence excitation-emission matrix (EEM) have been widely used to examine sources, composition and biogeochemical cycling of DOM in aquatic systems (Coble, 1996; McKnight et al., 2001; Guéguen et al., 2005; Stedmon and Bro, 2008; DeVilbiss et al., 2016; Lu et al., 2023). However, previous studies mostly focused on the characterization of bulk DOM pool. Moreover, DOM has been shown to be highly heterogeneous in composition, optical properties, molecular size, and chemical/biological reactivity (Guo et al., 1996; Benner and Amon, 2015; Lin and Guo, 2020). Chemical and optical characterization in both bulk and size-fractionated DOM should provide new insights into the dynamics of DOM in river systems (Guo and Macdonald, 2006; Zou et al., 2006; Guo et al., 2009; Lin et al., 2021; Zhao et al., 2021) and its impact on the coastal marine environment (Guéguen et al., 2007;Guo et al., 2009;Bauer et al., 2013).

The Mississippi River is one of the largest world rivers and an important source of freshwater and DOM for the Gulf of Mexico, ranking approximately seventh in DOC flux among the world rivers (Raymond and Spencer, 2015). Like other large rivers such as the Changjiang River, the Mississippi River is subject to extensive human disturbance with a number of studies reporting on the occurrence, composition, fluxes, and dynamic cycling of DOM and its impact on the coastal ocean (Bianchi et al., 2004; Dagg et al., 2005; Duan et al., 2007a, 2007b; Stolpe et al., 2010; Shen et al., 2012; Hanley et al., 2013; Cai et al., 2015; Duan et al., 2017; Stackpoole et al., 2017). The Pearl River, in contrast, is a small forest, black water river with relatively less anthropogenic influences but high DOM yields (Duan et al., 2007b; Stolpe et al., 2010; Cai et al., 2016), which, collectively, may have a large impact on estuarine and coastal ecosystems (Bianchi et al., 1998). These two rivers are distinct in drainage basin areas and human impacts, yet both export at close proximity to the Gulf of Mexico, making them model rivers for a comparative study on the composition, sources, and fluxes of DOM between large and small rivers as well as their relative role in the contribution of terrestrial DOM to the Gulf of Mexico. Further, systematic studies with multi-year time-series sampling scheme on the characterization of CDOM, FDOM, and colloidal DOM of large rivers such as the Mississippi River and comparison to small rivers such as the Pearl River remain scarce.

In the present study, longer-term time series samplings were carried out between January 2009 and August 2011 to examine temporal variability in the abundance, size partitioning and optical properties of DOM in the lower Mississippi River, Louisiana and the Pearl River, Mississippi. The study period included the Mississippi River flood in 2011 which resulted in enhanced DOC flux to the northern Gulf of Mexico and contributed to its waters changing in the summer from a net sink to a net source of CO_2 to the atmosphere (Bianchi, 2013). Measurements included bulk DOC, total dissolved nitrogen (TDN), colloidal and LMW-DOM isolated using ultrafiltration, CDOM absorption using UV–vis spectroscopy, and fluorescence EEM spectra using fluorescence spectroscopy, as well as EEM-PARAFAC analysis. Our main objectives were to 1) characterize composition and chemical/optical properties of DOM in time-series samples from each river; 2) examine the interrelationship between DOM properties and hydrological regime, 3) elucidate the similarity and differences in DOM properties between more pristine and human-impacted rivers and between large and small rivers and the influence of flood events, and 4) provide baseline datasets to identify potential DOM proxies for tracking future changes in DOM biogeochemistry and impacts on coastal marine ecosystems in response to climate and environmental change.

2. Methods

2.1. Study sites

The Mississippi River is the largest river in North America (~3770 km, average flow rate of 19,218 m^3/s), with a drainage basin area of ~3,220,000 km^2 covering about 40 % of the contiguous United States and a small part of Canada (Meade et al., 1990; Milliman, 1992). Cropland takes about 58 % of its drainage basin, making the Mississippi River basin one of the most productive farming regions in the world (Goolsby and Battaglin, 2001). In addition, dam systems and flood-control levees have restrained the river and reduced sediment discharge to the Gulf of Mexico (Meade et al., 1990), influencing the biogeochemical cycling of organic carbon species in the lower river (Duan et al., 2013; Cai et al., 2020).

The Pearl River is a small black-water river that drains the east-central Mississippi and southeastern Louisiana into the northern Gulf of Mexico. It is 790 km long and ranks as a 3rd order stream with an average discharge of 260 m^3/s and a total drainage area of about 22,690 km^2 (Table S1) which is only <1 % of the Mississippi River's drainage base area. In contrast to the Mississippi River, agricultural region in the Pearl River basin represents only ~27 % of the land use and natural forests cover about 43 % of the drainage basin (http://www.deq.state.ms.us). Differences in hydrological and other parameters between the Mississippi River and the Pearl River are listed in Table S1.

2.2. Sample collection

Monthly water samples were collected from the lower Mississippi River near the U.S. Geological Survey (USGS) hydrological station at Baton Rouge, Louisiana (30°26′17.01"N, 91°11′33.14"W) from January 2009 to August 2011 (Fig. 1). The Pearl River water samples were collected at Bogalusa (PRB), Louisiana (30°47′30"N, 89°49′20"W) and at the East Pearl River at Stennis Space Center (SSC), Mississippi (30°20′55.52"N, 89°38′28.74"W). Selected samples were also collected from the West Pearl River (PRW), Mississippi (30°23′10.92"N, 89°44′13.08"W) (Fig. 1). The sampling dates, locations and hydrographic parameters are listed in Tables S2 and S3. Discharge data for the lower Mississippi River at Baton Rouge and the lower Pearl River at Bogalusa hydrological stations were acquired from the USGS national water information system (http://waterdata.usgs.gov/nwis/rt).

Large volumes of surface waters were directly pumped peristaltically from the rivers and filtered in situ through an online filtration setup with a 0.4 μm Memtrex polycarbonate cartridge (GE Water & Process Technologies). About 40 L of the <0.4 μm filtrate was collected for ultrafiltration in acid cleaned HDPE containers after triple rinsing with filtrate (Guo and Macdonald, 2006; Cai et al., 2015). In addition, aliquots of filtered waters were collected in amber glass vials for the measurements of DOC, dissolved inorganic carbon (DIC), TDN, CDOM and FDOM. Samples were kept in an iced cooler and transported back to the lab

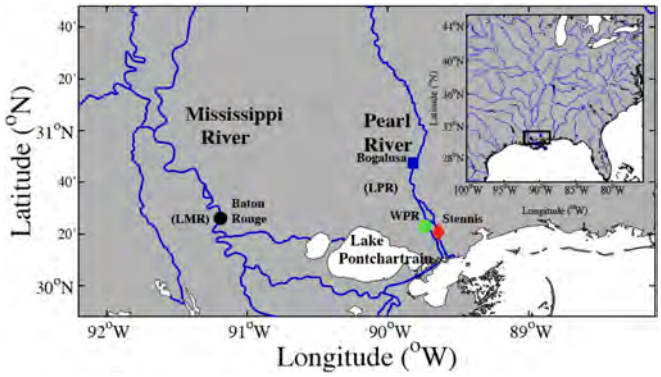

Fig. 1. Sampling locations in the lower Mississippi and Pearl Rivers. Red diamonds represent Pearl River samples taken at the Stennis Space Center. Blue squares represent Pearl River samples from Bogalusa, Louisiana. Green circles represent samples collected at the West Pearl River. (For interpretation of the references to color in this figure legend, the reader is referred to the web version of this article.)

within 2–3 h of collection for further processing. DOC samples were acidified to a pH of ≤2 (Zhou and Guo, 2012). Measurements of DOC, DIC, TDN, CDOM and FDOM were usually carried out within one week. Water temperature and conductivity were measured with an YSI sonde at the time of sample collection (Tables S2 and S3).

2.3. Ultrafiltration

A cross-flow ultrafiltration system equipped with a spiral-wound cartridge with a nominal molecular weight cutoff of 1 kDa was used to isolate colloidal or high-molecular-weight-DOM (HMW-DOM) and to examine the partitioning of DOM between the <1 kDa (or LMW) and the >1 kDa colloidal or HMW phases. Colloids here are operationally defined as the 1 kDa - 0.4 μm size fraction and were quantified using the ultrafiltration permeation model (Cai and Guo, 2009; Guo and Santschi, 2007).

Specifically, large volumes (20 L) of water samples were ultrafiltered, allowing the collection of time-series permeate samples at different concentration factors (CF) to fit the ultrafiltration permeation model:

$$lnC_p = ln\left(P_c \times C_f^0\right) + (1 - P_c) \times ln(CF)$$

where C_p is the DOC concentration of the time-series permeate samples, P_c is the permeation coefficient of permeable DOC, defined as the ratio of C_p (permeate concentration) to C_f (the feed concentration) at any given time, and C_f^0 is the initial feed concentration of the permeable DOC or LMW-DOC. The LMW-DOC concentration (C_f^0) and thus the colloidal OC abundance in a specific water sample was then derived from the above equation and the initial bulk DOC concentration (Guo and Santschi, 1996; Belzile and Guo, 2006).

2.4. Measurements of DOC, DIC and TDN

Concentrations of DOC, DIC, and TDN were measured with a Shimadzu TOC-V total organic carbon analyzer interfaced with a nitrogen detector using the high temperature combustion method (Guo et al., 1995; Cai et al., 2015). Calibration curves were generated each analytical day before sample analysis. The detection limit was 0.8 μM for DOC (Guo and Santschi, 1997). The precision was better than 2 % in terms of coefficient of variation (cv). Ultrapure water, working standards, and certified DOC samples (from University of Miami) were measured every eight samples to ensure data quality (Zhou and Guo, 2012).

2.5. Measurements of UV–vis absorption

The UV–vis absorption spectra were measured on a Cary 300 Bio UV–visible spectrophotometer using a 1-cm path-length quartz cuvette over 200–1100 nm with 1 nm increments (Zhou et al., 2013). The water blank was subtracted, and the instrument baseline drift, temperature, and refractive index effect were corrected by subtracting the average absorbance between 650 and 800 nm (Helms et al., 2008). Samples with absorbance values higher than 0.02 at 260 nm were diluted before analysis to minimize both reabsorption and inner filter effects (Zhou et al., 2016a). Values of specific UV absorbance at 254 nm ($SUVA_{254}$) were calculated as $SUVA_{254}$ = A(254 nm)/DOC, which is a measure of aromaticity, with a dimension of m^{-1}/(mg-C/L) or m^2/g-C (Weishaar et al., 2003). Spectral slope values were calculated using non-linear regression over wavelength interval between 275 and 295 nm and have been used as an indicator of CDOM molecular weight in natural waters (Helms et al., 2008).

2.6. Measurements of fluorescence EEMs and PARAFAC analysis

Fluorescence EEM spectra were obtained with a Shimadzu RF-5301PC scanning spectrofluorometer and a UV-grade quartz cuvette (10 mm light path) running the Panorama fluorescence 1.1 software (LabCognition, Dortmund, Germany). For each fluorescence EEM, emission spectra were recorded and concatenated over the range of 240–680 nm with 1 nm steps under excitation from 220 nm to 400 nm with 2 nm steps. Scans of ultrapure water were subtracted from the sample spectra before EEM contour plots were generated. Fluorescence intensities were expressed in quinine sulfate equivalents (QSE) in ppb (Coble, 1996; Zhou et al., 2013). In addition to calibrations using quinine sulfate, emission correction spectra were generated using rhodamine B and barium sulfate with the Shimadzu correction package and applied to the EEM spectra for correction of instrument bias (Zhou et al., 2013). Careful calibrations are needed to address instrument specific biases as indicated by comparison studies (Cory et al., 2010; Murphy et al., 2010).

The biological index (BIX) was calculated as the ratio of fluorescence intensity at 380 nm to that at 430 nm under Ex = 310 nm, which is indicative of autochthonous DOM (Huguet et al., 2009). Humification index (HIX) was calculated from the EEM by the ratio of the integration of fluorescence intensity between the wavelength range of 300–345 nm and 435–480 nm at Ex = 254 nm (Zsolnay et al., 1999).

PARAFAC analyses were performed in MATLAB (Mathworks, R2018b) using the DOMfluor and drEEM toolbox (Murphy et al., 2013; Stedmon and Bro, 2008; Lin and Guo, 2020). Models were constrained to nonnegative values, and three outliers were removed in the outlier tests. Normalization was done before developing the model. The results were validated using split-half analysis (Andersen and Bro, 2003; Stedmon et al., 2003). The percentage of explained variations in the validated model reached to 99.27 %. Relative percentage of PARAFAC components were calculated as Fmax of the component normalized to the sum of Fmax of all major PARAFAC components.

2.7. Statistical analysis

Statistics analyses were done in MATLAB (Mathworks, R2018b) including correlations, one-way ANOVA test, and *t*-test. Significance levels of correlations were examined using one-way ANOVA tests. *P*-values <0.01 were considered statistically significant. Pearson's correlation coefficients were used to examine the relationships between different parameters.

3. Results and discussion

3.1. Variations in discharge, physicochemical parameters and bulk DOC

The monthly sample collection covered a large range of discharge conditions in the two rivers. Discharge in the lower Mississippi River (LMR) at Baton Rouge ranged from 7538 to 40,012 m^3/s, with most prominent peak during a flood in May 2011 (Table S2, Fig. 2). The discharge during this historical flood event (40,012 m^3/s) was 108 % higher than the long-term average discharge (19,218 m^3/s, Table S1). In contrast, significantly smaller discharge ($p < 0.0001$) was found in the lower Pearl River (LPR) at Bogalusa, ranging from 37 to 2010 m^3/s (average 338 ± 494 m^3/s), with the highest flow at a flood event in April 2009 (Table S3, Fig. 2).

Temperature displayed strong seasonal cycles in both LMR (19.5 ± 9.8 °C) and LPR (22.1 ± 8.0 °C) with low values in winter and high in summer/early fall. Specific conductance, a measure of total dissolved solutes, in the river water was on average significantly greater in the LMR (360.8 ± 65.8 μS/cm) than in the LPR (80.9 ± 47.3 μS/cm) and was negatively correlated to discharge in both the rivers ($R^2 = 0.61$, $p < 0.01$ in LMR, $R^2 = 0.20$, $p < 0.05$ in LPR). Lowest values of specific conductance were measured during the peak flood discharge (Tables S2 and S3) indicating strong dilution effect during high river discharge periods. Rivers transport carbon in dissolved form as DOC and DIC. Concentrations of DIC were on average significantly greater in the LMR (2366 ± 436 μM) than in LPR (349 ± 150 μM) (Tables S2 and S3). These DIC results are similar to those reported for both rivers at different sampling time periods (Cai et al., 2013, 2015). Noticeably, the average DIC concentration in the LMR is as high as those in global oceans (Broecker and Peng, 1982), mostly due to the presence of limestone in the Mississippi River basin. Some of the highest values occurred during low flow conditions in both rivers resulting from increased groundwater proportion. DIC showed a general decreasing trend with increasing discharge in the LMR, while it was elevated and variable at low discharge conditions (<500 m^3/s) but displayed an increasing trend at higher discharge levels. In the LPR, the average DIC concentration was much lower than that in the LMR. Furthermore, although DIC decreased in general with increasing discharge below 200 m^3/s, its DIC concentration reached a stable low value under discharge higher than 200 m^3/s. TDN concentrations were on average higher in the LMR (118.5 ± 39.1 μM) compared to the LPR (30.2 ± 8.6 μM) (Tables S2 and S3); however, TDN was highly variable in the LMR compared to LPR, likely due to its diverse dissolved N sources, both natural and anthropogenic. In the LMR, nitrate was the major TDN species (61 %) with principal source from the agricultural lands (Goolsby and Battaglin, 2001); in comparison, anthropogenic impacts on nutrients are less in the PR.

Concentrations of DOC in the LMR ranged from 236 to 388 μM, with an average of 306 ± 40 μM during the sampling period corresponding to the river discharge that varied seasonally and over a large range (7538 to 40,012 m^3/s) between January 2009 and August 2011 (Table S2, Fig. 2); generally, monthly sampling indicated elevated DOC concentrations with peaks in river discharge with DOC positively correlated to discharge ($p < 0.001$, $r^2 = 0.38$, Fig. 3) indicating strong hydrological control on DOM dynamics; knowledge of such hydrological linkage is important to improve monitoring and modeling of riverine carbon fluxes to the coastal ocean (Li et al., 2017; D'Sa et al., 2023). In the LPR, DOC concentrations ranged from 225 to 1121 μM with an average of 543 ± 206 μM (Table S3, Fig. 2) showing significant positive correlation with discharge ($p < 0.0001$, $r^2 = 0.55$, Fig. 3) which varied over a much smaller discharge range (37 to 2010 m^3/s) compared to the LMR. Average DOC concentrations in the LPR are higher than those reported

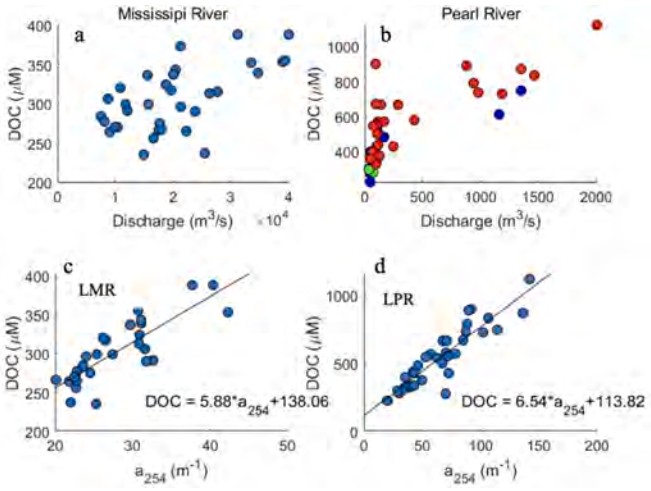

Fig. 3. Relationships between discharge and concentration of DOC (a, b) and between CDOM (in terms of a_{254}) and DOC (c, d) in the lower Mississippi and Pearl Rivers (see color codes in Fig. 1).

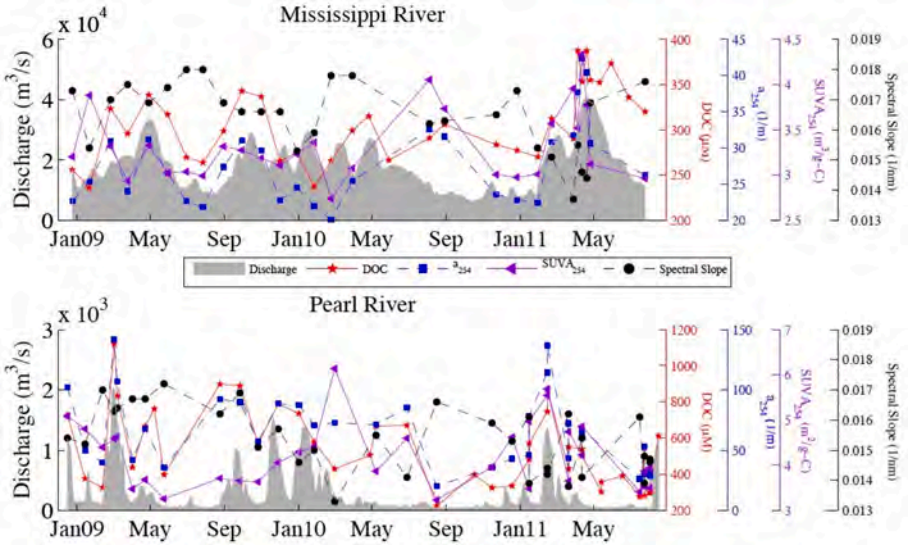

Fig. 2. Variations in discharge, dissolved organic carbon (DOC), absorption coefficient at 254 nm (a_{254}), specific UV absorbance at 254 nm ($SUVA_{254}$) and spectral slope between 275 and 295 nm ($S_{275–295}$) in the lower Mississippi and Pearl Rivers between January 2009 and September 2011.

for similar smaller rivers in the northern Gulf of Mexico such as the Mobile River (Spencer et al., 2012) or the Trinity River (Warnken and Santschi, 2004).

Significantly lower DOC concentration ($p < 0.0001$) observed in the LMR compared to the LPR is consistent with the land types in the drainage basins of the two rivers. The Mississippi River receives less DOC input from cropland, while the major forest land type in the Pearl River basin leads to higher DOC yields (Mattsson et al., 2005). DOC in the LMR also showed smaller seasonal variability than the Pearl River (as indicated by its smaller cv, 13 %) that could be attributed to its large river volume and capacity to bear large quantities of upstream inputs, thus resulting in integrated and less variable signals (Duan et al., 2007a). In addition to the difference in land type, a larger number of dams and levees along the Mississippi River lead to a longer water residence time and hence a higher loss of DOM (Duan et al., 2013; Évrard et al., 2023). In contrast, DOC in the LPR has larger temporal variability, as indicated by its higher cv (38 %), suggesting its major DOM sources from local input of soil DOM and plant litters and controlled by the highly variable hydrological conditions (Duan et al., 2007a; Malcolm and Durum, 1976).

While the average DOC concentration in the LMR (306 ± 40 μM) is much lower than that in the LPR (543 ± 206 μM), the opposite holds true for their average DIC concentrations (Tables S2 and S3). The average DOC:DIC ratio was 0.13 for the LMR, contrasting with the substantial ratio of 1.56 in the LPR. This suggests that river export of DOC from the LMR to the Gulf of Mexico accounted for only ~13 % of its DIC export flux, but DOC export from the LPR was up to 156 % of its DIC export or mostly in the form of DOC. Despite the fact that the average freshwater discharge from the LMR was 74 times that from the LPR (Table 1), the average DOC concentration in the LMR was only ~50 % of that in the LPR during the sampling period. In other words, average DOC export flux from the LMR was only about 37 times of the DOC flux from the LPR. In terms of DOC production (in mass-DOC) per sq. meter of the drainage basin area per year, the DOC yield from the Pearl River basin (~1.9 g-C/m^2/yr) is about 3 times that from the Mississippi River basin (0.6 g-C/m^2/yr). Therefore, DOC export fluxes from small pristine, black water rivers should not be ignored (Liao et al., 2019).

3.2. Variations in CDOM optical properties and flood events

CDOM optical properties, including absorption coefficient at 254 nm (a_{254}), specific UV absorbance at 254 nm ($SUVA_{254}$), and spectral slope ($S_{275–295}$) values, show large variability over the sampling period in the two rivers (Fig. 2; Tables S2 and S3). Overall, a_{254} for both rivers showed similar trends to that of DOC concentrations as a function of river discharge (Fig. S1). Strong relationships were observed between a_{254} and DOC both in the LMR ($r^2 = 0.69$, $p < 0.0001$) and the LPR ($r^2 = 0.87$, $p < 0.0001$, Fig. 3c, d). This significant correlation between a_{254} and DOC makes CDOM an excellent proxy for DOC in these two rivers, suggesting that upon absence of DOC measurement, a_{254} could be used to estimate DOC concentration although specific slope values are different for different rivers. Indeed, strong correlation between CDOM and DOC extending into the estuaries and shelf waters influenced by the MR has been used to estimate DOC from ocean color satellite-derived CDOM to study DOM dynamics and fluxes in the coastal ocean (Tehrani et al., 2013; Liu et al., 2019).

Table 1
Characteristics of major fluorescence DOM components in the combined lower Mississippi River and Pearl River identified by PARAFAC analysis.

Fluorescent Component	Excitation wavelength (nm)	Emission wavelength (nm)	Description
Component – 1	250	451	UVC humic-like DOM
Component – 2	366	467	Visible humic-like DOM
Component – 3	<250, 328	417	Terrestrially derived organic matter
Component – 4	276	376	Amino acids from biological production

In the LMR, a_{254} ranged from 20.1 m^{-1} in March 2010 to 42.3 m^{-1} in May 2011 (average 27.9 ± 5.7 m^{-1}) and $SUVA_{254}$ varied from 2.74 m^2/g-C in March 2010 to 4.34 m^2/g-C^1 in May 2011 (average 3.32 ± 0.39 m^2/g-C, Fig. 2). Spectral slope values ($S_{275–295}$) ranged from 0.0137 to 0.0180 nm^{-1} (average 0.0165 ± 0.0116 nm^{-1}) in the LMR showing a decreasing trend with increasing discharge ($p < 0.02$, Table S2). The Mississippi River flood of spring 2011 was one of the largest on record (waterdata.usgs.gov) at a scale that rivaled the great flood of 1927 (see also discussion in section 3.1). The floods were triggered by two large storms that deposited record levels of rainfall on the drainage basin in April 2011, which, combined with spring snowmelt, contributed to record discharge in May 2011 (Fig. 2, Table S2). DOC concentrations in the LMR peaked to their highest levels in May 2011 (388 μM), with peaks in CDOM or a_{254} (42.31 m^{-1}), $SUVA_{254}$ (4.34 m^2/g-C) and lowest value of $S_{275–295}$ (0.0144 nm^{-1}) suggesting greatest aromaticity and molecular size in the bulk DOM pool associated with this extreme flood event over the study period. The low value of spectral slope suggest that photo-oxidation may not contribute much to changes in the molecular structure of the DOM pool during high flow seasons in large rivers. Such anomalously high discharge events have been linked to large DOC fluxes into estuaries and coastal waters (Liu et al., 2023) or to enhanced cross-shelf export of terrigenous DOC in the northern Gulf of Mexico (Fichot and Benner, 2014) with implications for coastal biogeochemical processes and carbon budgets (Ward et al., 2017).

In the LPR, a_{254} ranged from 20.1 m^{-1} in September 2010 to 142.2 m^{-1} in April 2009 (average 66.4 ± 31.4 m^{-1}) and $SUVA_{254}$ varied from 3.23 m^2/g-C in September 2010 to 6.14 m^2/g-C in March 2010 (average 4.24 ± 0.72 m^2/g-C). Similarly, the April 2009 flood event in the Pearl River resulted in the highest DOC concentrations (1121 μM) and a_{254} (142.2 m^{-1}), with elevated $SUVA_{254}$ (4.59 m^2/g-C) and relatively higher $S_{275–295}$ (0.0163 nm^{-1}). A second flood event in March 2011 also resulted in elevated DOC concentrations (870 μM) and a_{254} (136.6 m^{-1}) and highest $SUVA_{254}$ (5.68 m^2/g-C) and relatively low $S_{275–295}$ (0.0142 nm^{-1}). Differences in DOM characteristics between different flood events suggest that specific season, flood distribution, and flushing pathways all play a role in modifying the aromaticity and molecular size distribution of the DOM pool in the river. Such flood impacts on DOM dynamics have been reported for other rivers with similar discharge conditions such as the Arno River in the Mediterranean (Brogi et al., 2020).

Similar to DOC concentration, significantly lower a_{254} ($p < 0.0001$) and $SUVA_{254}$ ($p < 0.0001$) were found in the LMR compared to the LPR, suggesting the presence of less aromatic DOM in the LMR (Weishaar et al., 2003), which can be linked to the land type of the their drainage basins. In addition, higher DOC, a_{254} and $SUVA_{254}$ were found during flood events in both rivers (Fig. 2), suggesting a release of DOM with higher aromaticity during high flow. Greater proportion of hydrophobic carbon and more acidic DOM in surface soils leached during high flows likely lead to changes in DOM during different flow conditions (Cronan and Aiken, 1985; Yano et al., 2005a; Yano et al., 2005b). In contrast, in the LPR, $S_{275–295}$ ranged from 0.0133 to 0.0172 nm^{-1} (0.0153 ± 0.0107 nm^{-1}) (Table S3), without significant correlation ($p > 0.1$) between $S_{275–295}$ and discharge, likely attributed to its unique and less varied DOM sources in the Pearl River basin.

The lower aromaticity and smaller DOM size observed in the LMR also suggest lower forest coverage, greater photochemical reactions, and stronger biodegradation of DOM during its extended downstream transport. Indeed, in situ processing of DOM has been linked with decreased DOM aromaticity and increased carboxyl carbon in DOM under exposure to bacterial decomposition and photochemical oxidation (Engelhaupt and Bianchi, 2001; Osburn et al., 2001).

The relationships between DOC and a_{254} in the LMR and LPR showed positive intercepts when a_{254} or CDOM approaches zero (Fig. 3c, d). This

intercept value could be associated with the average abundance of non-chromophoric DOC in a specific aquatic system (Spencer et al., 2012; Zhou et al., 2016a). Accordingly, the non-chromophoric fraction of DOC in the LMR and LPR were ~ 138 μM and ~ 114 μM, representing ~46 % and ~ 21 % of their corresponding bulk DOC, respectively. The higher amount of non-chromophoric DOC in the LMR agrees well with its lower aromaticity observed and longer water residence time and thus extensive degradation/modification of aromatic DOM in the river (Engelhaupt and Bianchi, 2001; Osburn et al., 2001; Chen and Jaffé, 2016). Another possible contributing factor to the different non-chromophoric DOC levels is the difference of DOM sources between the two rivers. In the LMR, there is relatively more aquagenic DOM present (see discussion below) while more terrestrial DOM that is high in humic-like materials and is more chromophoric is introduced to the Pearl River (Stolpe et al., 2010; Zhou et al., 2016b). These differences in DOM quantity and quality from the two rivers are likely to impact its reactivity and fate in the coastal and shelf waters (Bauer et al., 2013).

3.3. Fluorescence indices/components of bulk DOM and linkages to river discharge

Examples of two typical fluorescence EEM spectra of samples collected from the LMR and LPR (Fig. S2) generally indicate similar EEM patterns. The LMR showed signatures of humic-like fluorescent DOM (Peaks A and C) with additional protein-like material signals. The LPR also showed predominant humic-like fluorescent signatures (Peaks A and C) but greater intensity and more red-shifted indicating greater aromaticity of the fluorescent DOM, with protein-like peaks relatively less important compared to those in the LMR.

The biological index (BIX) in the LMR ranged from 0.61 to 0.77 with an average of 0.67 ± 0.04 (Fig. 4a), and decreased with increasing discharge ($P < 0.00001$, $r^2 = 0.73$), while BIX in the LPR (Fig. 4b) ranged from 0.45 to 0.66 (average 0.55 ± 0.06), also negatively correlated with discharge ($P < 0.00001$, $r^2 = 0.48$). The decreasing trend of BIX with increasing discharge in the two rivers suggests the dilution of autochthonously produced DOM during higher flow seasons. Significantly higher BIX ($P < 0.00001$) in the LMR indicated its higher contribution of autochthonous DOM and is consistent with higher chlorophyll-a abundance and stable carbon isotopic composition, δ^{13}C-DOC, observed in the LMR compared to LPR (Cai et al., 2013; Cai et al., 2015; Duan et al., 2007a). Indeed, prolonged water transition time due to dam and levee constructions in the LMR could cause increase in water clarity and increase the aquagenic DOM production, altering the composition of riverine DOM.

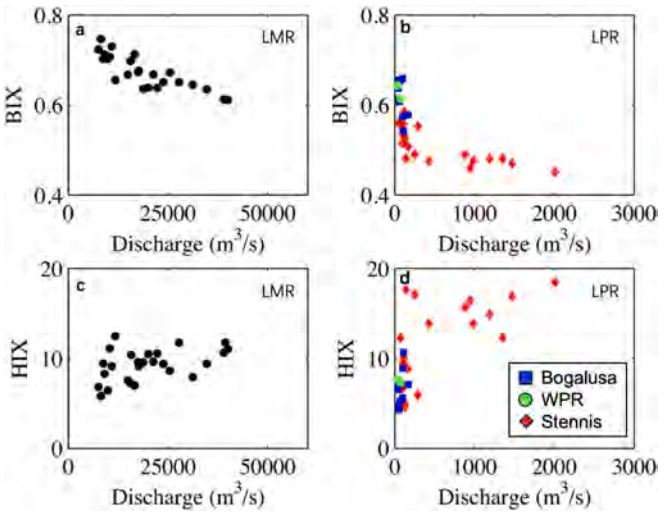

Fig. 4. Relations between discharge and fluorescence indices including biological index (BIX) and humification index (HIX) in the lower Mississippi River and Pearl River, showing a general increase in HIX but a decrease in BIX with increasing discharge in both rivers.

Humification index (HIX) ranged from 5.82 to 12.49 (9.27 ± 1.76) in the LMR (Fig. 4c) and increased with increasing discharge ($P < 0.05$, $r^2 = 0.21$). Similarly, values of HIX in the LPR ranged from 4.33 to 18.48 (9.69 ± 4.45) and showed an increasing trend with discharge ($P < 0.00001$, $r^2 = 0.50$) (Fig. 4d). The positive correlation between HIX and discharge indicated the introduction of more humified DOM from soil during flushing into the rivers in high flow seasons. Significantly higher $SUVA_{254}$ (see above section) and HIX values in the LPR ($P = 0.005$) suggest more humic-like material in the bulk DOM in the Pearl River from soil and plant litter (Lin et al., 2021). However, while both BIX and HIX had a general negative and positive correlation with discharge in both rivers, their variation trends are distinctly different between the LMR and LPR. For example, the HIX values reached a plateau under discharge higher than 200 m^3/s in the LPR, but this was less the case in the LMR (Fig. 4c, d). On the other hand, the BIX values decreased rapidly with increasing discharge and reached a stable low value when the discharge was >200 m^3/s. The unique variation trends in both HIX and BIX indicated that DOM sources are somewhat similar or less variable during high discharge time periods or flood seasons in the small river basin, the Pearl River, contrasting to the large river basin, the Mississippi River.

PARAFAC analysis when applied to a larger data set can effectively separate some chemical compounds apart into components (Stedmon et al., 2003). To statistically identify the major fluorescent DOM components in both rivers, PARAFAC analysis was applied to the combined EEM data of the monthly samples from both the rivers (Stedmon and Bro, 2008). As shown in Fig. S3 and Table 1, four major fluorescent components were identified. Component 1 (C1) had its maximum peak at Ex/Em 250/451 nm, likely associated with the Peak A (UV humic-like). Component 2 (C2) had Ex/Em maximum at ~366/467 nm, and could be identified as a visible humic- like component (Coble, 1996; Stedmon et al., 2003). The third component (C3) with Ex/Em at 250/417 and 328/417 nm seemed to be terrestrially derived organic matter, as suggested by Stedmon et al. (2003). While these riverine humic-like fluorescent components are being attributed to terrestrial origins, it has been shown that these same humic-like components are ubiquitous in diverse environments (Murphy et al., 2018; Wünsch et al., 2019; Kida et al., 2019). Component 4 (C4, Ex/Em ~276/376 nm) could be Peak T or a combination of Peak N and Peak T (Coble, 1996; Stedmon et al., 2003). The Peak N has been linked to some labile materials derived from biological production (Coble et al., 1998), while the Peak T is believed to have the indole ring structure of tryptophan and likely to originate from biological production in surface waters (Coble, 2007; Zhou et al., 2016a). Component 4, thus, was linked to amino acids and biological production.

The relative contribution of each component to the total fluorescence signal showed distinct patterns (Fig. S4). In the LMR, C1 (UV humic-like component) was positively correlated with discharge under normal seasonal discharge conditions (Fig. S4a). The C4 (protein-like component) in contrast showed a general decreasing trend with increasing discharge, suggesting a dilution of the authochthonous DOM under high discharge conditions or reduced primary production due to the high suspended particles in the high-discharge season. Meanwhile, in the LPR, all three components showed variability with no particular trends at discharge levels <200 m^3/s (Fig. S4d-f) suggesting different sources and processes influencing these fluorescent components under low flow conditions. However, with increasing discharge, C1 showed a negative trend while C2 exhibited a positive trend, suggesting different levels of mobilization with increasing discharge in the LPR. The C4 authochthonous component showed large variability at <200 m^3/s discharge levels, with lower values but no clear trends at higher discharge but at relatively lower levels compared to that in the LMR. Overall, the relations between discharge and the relative abundances of fluorescent DOM components showed different trends in the two rivers, consistent

with their unique DOM and hydrological characteristics with historical high discharge during 2009–2011 in the Mississippi River compared to 2006–2008 sampling years (Cai et al., 2015). The other factor causing their weak relationship may result from differences in fluorescent composition between the two rivers and between base flow and flood seasons. For example, the correlation between discharge and the relative abundances of fluorescent components in the LPR exhibited two groups: low discharge (<200 m^3/s) and high discharge (200–1400 m^3/s), with distinct slope values in their correlations. It should be noted that while many studies have examined changes in the relative fluorescent component abundances, care should be taken in their interpretation (Murphy et al., 2013) and future studies should consider obtaining high frequency samples under different discharge conditions in each river or, alternately, use the one-sample EEM-PARAFAC approach (Wünsch et al., 2017; Lin and Guo, 2020; Lin et al., 2023).

The flood events in the rivers not only resulted in elevated bulk DOM abundance, including DOC and CDOM (or a_{254}), but also led to differences in fluorescence EEM characteristics (Fig. 5). The fluorescence intensity of fulvic- (peak C), humic- (peak A) and protein-like components all appear to increase with increasing discharge. However, relative intensities differ from before, during and after the flood events. In the LMR, the position of peak "A" slightly red-shifted to Ex/Em 250/455 nm during the flood in May 2011 as compared to other times of the year (Ex/Em ~240/~445 nm, Fig. 5). However, in spring/summer of 2011, component C1 (humic-like), decreased under extreme discharge conditions, indicating reduced mobilization of this component during flood seasons. In contrast, component C2 (visible humic-like) showed an increasing trend under flood conditions suggesting different sources of these two humic-like components. Changes in the fluorescence indices (low BIX and elevated HIX; Fig. 4) further confirm large changes in both the quantity and quality of the DOM pool during large flood events in the LMR. Similar humic-like and protein-like fluorescent components were detected in the coastal and shelf waters influenced by the MR during sampling in 2009, with higher levels in the nearshore waters and decreasing offshore (D'Sa et al., 2016), indicating strong terrestrial signatures in the FDOM pool of the northern Gulf of Mexico.

The red shift of peak position was also found in the LPR during its flood in April 2009 from Ex/Em ~240/~455 nm to 338/459 nm. Red-shift of peaks are usually linked to DOM with higher molecular weight (McKnight et al., 2001; Stedmon et al., 2003), thus, it seems that more higher molecular weight DOM were flushed from soil during flood events, in accordance with interpretation from colloidal DOM abundance observed and spectral slope values from UV–vis spectra (Tables S2 and S3) indicating a shift in humic moieties during large flood events. Such flood events which are predicted to increase in frequency with climate change will potentially increase the fluxes of terrestrial DOM magnitude and quality that have been reported to persist in coastal environments (Stolpe et al., 2014; Zhou et al., 2016b; Asmala et al., 2021) with implications to coastal ecosystems.

3.4. Variations in size-fractionated DOC, CDOM and FDOM

Size fractionated DOC: Concentrations of HMW-DOC in the LMR varied from 151 to 204 μM with an average of 176 ± 16 μM (cv = 9 %), comprising 52–64 % (58 ± 3 %) of the bulk DOC (Table S2). In the LPR, HMW-DOC ranged from 140 to 604 μM (327 ± 170 μM, cv = 52 %) representing 62–77 % (69 ± 5 %) of the bulk DOM (Table S3). Similar to DOC concentrations, both the HMW-DOC concentrations and its proportion in the bulk DOC in the LMR are significantly lower than those in the LPR (with $p < 0.01$ and $p < 0.0001$, respectively). Higher colloidal DOC abundances in the LPR are consistent with its higher CDOM abundance and higher $SUVA_{254}$ or aromaticity (Tables S2 and S3; Lin et al., 2021). In addition, both the HMW-DOC concentrations and the colloidal abundance had a larger variability in the LPR (52 %) compared to the LMR (9 %).

In general, concentrations of HMW-DOC increased with increasing discharge in the LMR ($p < 0.02$, $r^2 = 0.44$) and the LPR ($p < 0.05$, $r^2 = 0.57$), suggesting flushing of more HMW-DOC from surface soil during higher discharge (Nugyen et al., 2010). Nevertheless, during the freshet season in April 2009, the concentration of HMW-DOC in the LPR increased, but not as high as one would expect from the relationship between HMW-DOC and discharge at discharge <500 m^3/s. This

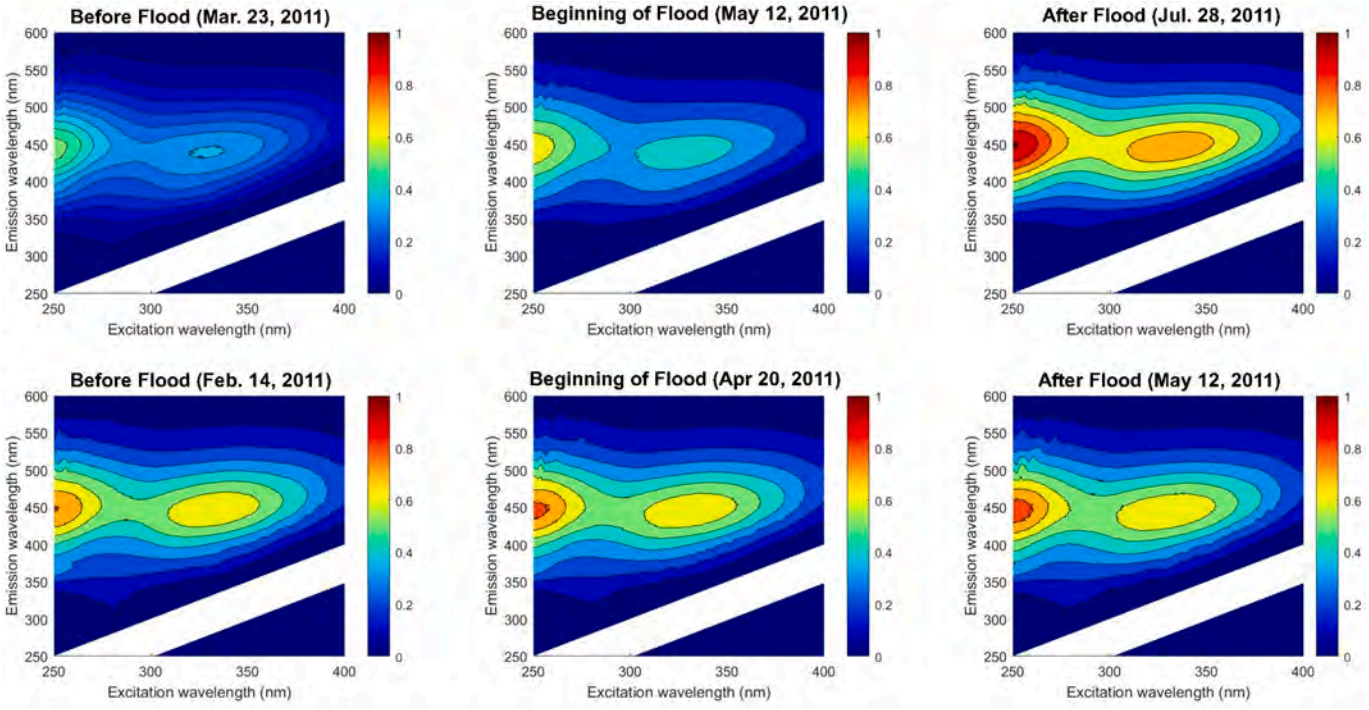

Fig. 5. Examples of fluorescence EEM spectra (relative units) of water samples before, beginning of, and after a flood event from the lower Mississippi River (upper panels) and the Pearl River (lower panels).

suggests a limited supply of HMW-DOC from the leaching of surface soil during river freshet and thus a dilution effect in the LPR, although the HMW-DOC concentration increased in general with discharge. This variation trend is similar to that observed for HIX values in the LPR.

Size fractionated CDOM: Significantly higher spectral slope ($p < 0.0005$) in the LMR suggest that the apparent DOM molecular weight in the bulk DOM pool was lower (Helms et al., 2008), matching its lower colloidal or HMW-DOM size fraction as determined via ultrafiltration. Land use could also play a role in controlling these different DOM characteristics in the two rivers. DOM export from agricultural soil has been found to have more LMW-DOM components and a decrease in soil humic substances (Dalzell et al., 2005; Guo and Chorover, 2003). In the lower Mississippi River basin, high percentage of croplands (~58 %) also likely contributed to the decrease in DOM molecular weight and aromaticity in the LMR.

In the ultrafiltration-derived size-fractionated DOM samples from the two rivers, spectral slope values showed a consistent trend, where the <1 kDa LMW-DOM fractions had consistently higher spectral slope values compared to both the bulk DOM, which had intermediate spectral slope values, and the >1 kDa HMW-DOM, which had lowest spectral slope values (Fig. 6). This robust inversed correlation between spectral slope and DOM molecular weight further supports the use of spectral slope as an indicator of DOM molecular weight in aquatic environments (Helms et al., 2008). As an example, for the LMR sample (30 July 2009), the relatively high bulk DOM spectral slope (0.018 nm^{-1}) was also associated with the elevated value for the LMW-DOM size-fraction (Fig. 6) indicating an overall shift to more LMW-CDOM pool, likely due to enhanced photobleaching during the summer under low-flow river conditions. This also suggest substantial photobleaching could occur within the river and during its transit to the coastal ocean, where DOM is further subjected to biogeochemical transformations. Similarly, in the case for the PR sample, there was a decrease in spectral slope in the HMW fraction compared to the bulk DOM although less significant compared to those in the LMR (Fig. 6), likely due to the greater HMW fraction in the bulk DOM pool in the LPR (Table S3).

Size fractionated FDOM properties: The fluorescence EEMs of bulk (<0.45 μM), LMW- (<1 kDa), and HMW-DOM (1 kDa - 0.45 μm) of selected samples are shown in Fig. 7. The humic-like fluorescence signature (peaks A and C) observed in the bulk DOM and the LMW- and HMW-DOM fractions for this study are similar to previously reported data observed in river and coastal regions (Coble, 1996). However, the maxima of these peaks are shifted to shorter wavelengths for the LMW-DOM fraction compared to bulk DOM. Protein-like signatures were also observed in the bulk DOM and LMW-DOM fraction (Fig. 7). These results

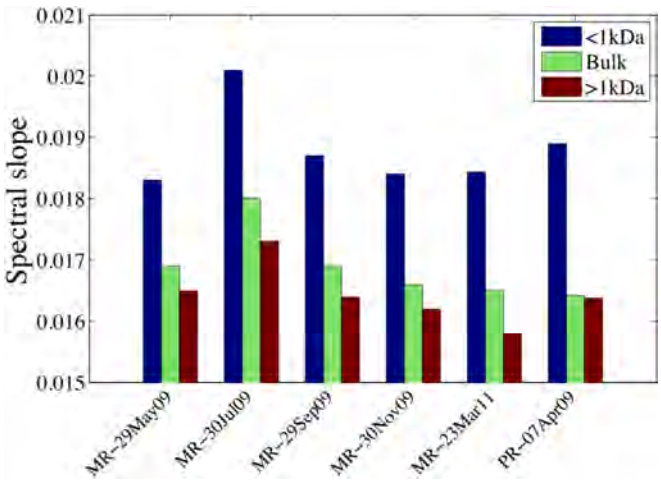

Fig. 6. Examples showing the variations in spectral slope values ($S_{275-295}$) in the <1 kDa LMW-DOM, bulk DOM, and the >1 kDa HMW-DOM size-fractions isolated using ultrafiltration.

are generally representative of the three distinct classes of fluorophores (fulvic-, humic- and protein-like) signatures.

Compared to the bulk sample, fluorescence signatures of LMW-DOM seemed to have higher relative importance of UV-humic like DOM (peak A, ~ Ex/Em 240/460 nm), as opposed to visible terrestrial humic-like DOM (peak C, Ex/Em 340/450 nm), and also relatively more tyrosine-like materials (peak B, Ex/Em ~230,275/310 nm). In addition, while the primary peak in the LMW-DOM was mostly at Ex/Em of 240/460 nm, the HMW-DOM exhibited not only peak A but also peak C with Ex/Em of 340/450 nm. Another notable difference in HMW-DOM composition between the two rivers is that peak C was the primary fluorescent component in the HMW-DOM pool in the LMR, whereas peak A was identified as the major fluorescent component in the LPR (Fig. 7).

Similar to other optical properties, the BIX values were found to be higher in the LMW-DOM fraction but lower in the HMW-DOM fraction as compared with the bulk DOM (Fig. 8). In contrast, HIX were found lower in the LMW fraction and higher in the HMW fraction (Fig. 8). These observations suggest partitioning of distinct DOM in specific size fractions, with DOM from autochthonous sources more partitioned to the LMW size range and more humified DOM preferentially present in the HMW size range (Lin et al., 2021). Such characterization of the optical properties of size fractionated DOM in both large and small rivers could improve understanding the biogeochemical cycling and fate of an important DOM pool in the coastal ocean (Guo and Macdonald, 2006; Guo et al., 2009; Lu et al., 2023).

4. Conclusions

The Mississippi River, one of the largest world rivers and the largest in north America, is a major source of DOM to the northern Gulf of Mexico. While the quantity of DOC has been reported for numerous rivers worldwide, the quality of riverine DOM has been scarce. Based on chemical and optical characterization of longer-term monthly water samples from the lower Mississippi River and Pearl River between January 2009 and August 2011, the following findings have been deduced.

DOM in Mississippi River waters showed lower abundance, lower aromaticity, and lower fraction of colloidal or HMW-DOM, but higher non-chromophoric DOM. These DOM characteristics are consistent with the fact that the major land use in the lower Mississippi drainage basin is cropland and that there is a great number of dams and levees, which largely prolong the water residence time in the basin. In contrast, DOM in Pearl River waters was more aromatic with higher levels of HMW-DOM, and low abundance of non-chromophoric DOM, showing major DOM sources from local surface soil and plant litters with less degradation. The differences in DOM sources, hydrological conditions, and anthropogenic influences between the lower Mississippi River and Pearl River basin played an important role in controlling the optical properties and characteristics of DOM in river waters and their influences on the northern Gulf of Mexico. In turn, optical properties and CDOM measurements could provide valuable insights into understanding DOM dynamics in different river basins. Examination of optical properties of DOM in size-fractionated samples from ultrafiltration revealed size partitioning of specific types of DOM. More humified DOM was associated with the higher abundance of the >1 kDa HMW-DOM fraction. Based on EEM-PARAFAC analysis, a four-component model could be validated for fluorescent DOM in both rivers. They include terrestrial humic-like, UV humic-like, degradation products of terrestrial organic matter, and protein-like DOM components. The characteristics of riverine fluorescent components are closely related to their sources and subsequent degradation and biogeochemical processes. During floods, humic-like DOM showed a red shift of peak position in fluorescence EEM spectra, linking to higher molecular weight humic-like material flushed from soil leachate and plant litters; thus, large flood events not only contribute to large increase in DOM quantity but also quality with implications to coastal carbon cycling. Although this study is limited to two

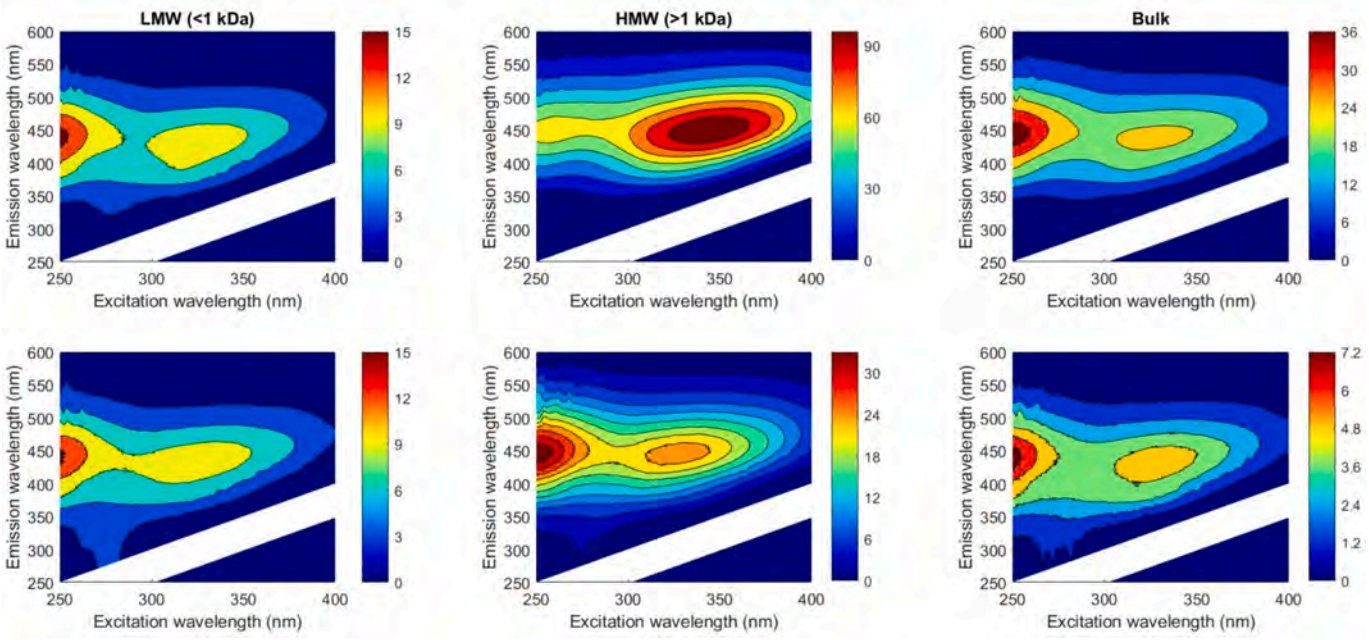

Fig. 7. Examples of fluorescence EEM spectra of different DOM size-fractions (bulk, LMW- and HMW-DOM) in water samples from the lower Mississippi (upper panels) and Pearl Rivers (lower panels) (Units in QSE).

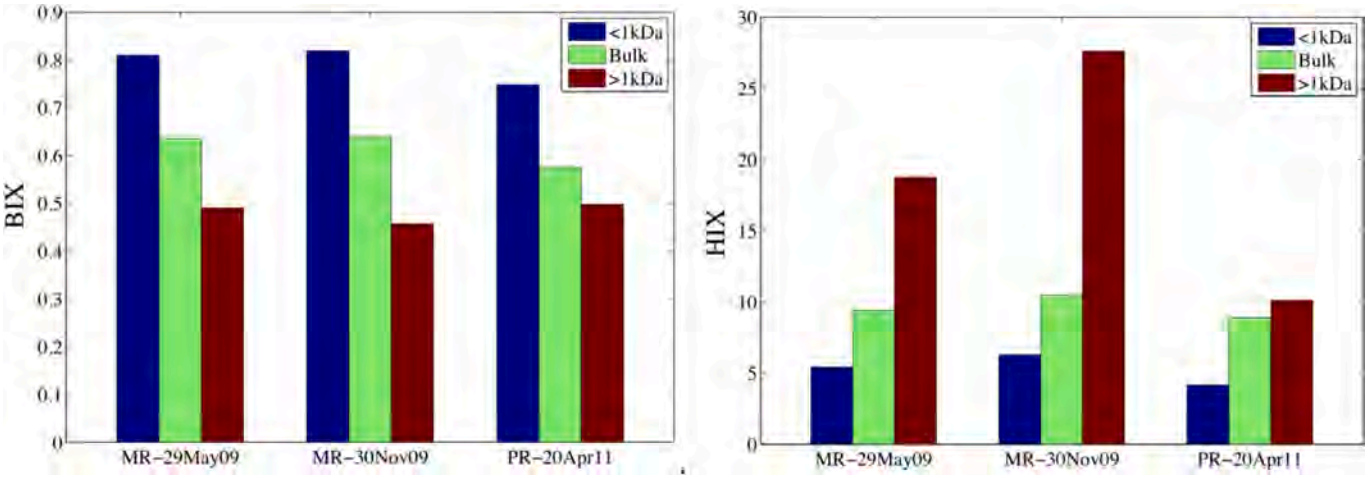

Fig. 8. Examples showing differences in fluorescence indices, including biological index (BIX) and humification index (HIX), between bulk DOM and size-fractionated DOM (the <1 kDa LMW and the >1 kDa HMW-DOM) in the LMR and the LPR.

rivers in the northern Gulf of Mexico, a better understanding of not only DOM quantity but also quality (CDOM absorption and fluorescence properties and size fraction) in these rivers should provide greater insights on coastal biogeochemical responses to hydrological events particularly under climate change.

CRediT authorship contribution statement

Zhengzhen Zhou: Writing – review & editing, Methodology, Investigation, Data curation. **Hui Lin:** Writing – review & editing, Visualization, Data curation. **Eurico J. D'Sa:** Writing – review & editing, Data curation. **Laodong Guo:** Writing – review & editing, Supervision, Methodology, Funding acquisition, Conceptualization.

Declaration of competing interest

None.

Data availability

Data will be made available on request.

Acknowledgments

We gratefully thank Xuri Wang, Dongjoo Joung, Kusumika Mitra, Huijun He, and Weifeng Yang for their assistance during sample collection and processing and the Editor and three anonymous reviewers for their constructive comments which greatly improved the presentation of our manuscript. Funding for the sampling was provided from NOAA through the Northern Gulf Institute (Projects #09-NGI-04 and 09-NGI-13) and National Science Foundation (OCE #0850957 to L.G.). This work was supported in part by Discovery and Innovation Grant Program from the University of Wisconsin-Milwaukee (101 × 405), National Science Foundation (award # 2204145), and Freshwater Collaborative of Wisconsin (UWSA.09 and SL3.27). E.D. acknowledges partial support

from a NASA grant (80NSSC22K0357).

Appendix A. Supplementary data

Supplementary data to this article can be found online at https://doi.org/10.1016/j.marchem.2024.104453.

References

Aiken, G.R., Hsu-Kim, H., Ryan, J.N., 2011. Influence of dissolved organic matter on the environmental fate of metals, nanoparticles, and colloids. Environ. Sci. Technol. 45 (8), 3196–3201.

Aitkenhead, J.A., McDowell, W.H., 2000. Soil C:N ratio as a predictor of annual riverine DOC flux at local and global scales. Glob. Biogeochem. Cycles 14 (1), 127–138. https://doi.org/10.1029/1999gb900083.

Andersen, C.M., Bro, R., 2003. Practical aspects of PARAFAC modeling of fluorescence excitation-emission data. Aust. J. Chem. 17 (4), 200–215. https://doi.org/10.1002/cem.790.

Asmala, E., Osburn, C.L., Paerl, R.W., Paerl, H.W., 2021. Elevated organic carbon pulses persist in estuarine environments after major storm events. Limnol. Oceanogr. Lett. 6, 43–50.

Bauer, J.E., Cai, W.-J., Raymond, P.A., Bianchi, T.S., Hopkinson, C.S., Regnier, P.A.G., 2013. The changing carbon cycle of the coastal ocean. Nature 504, 61–69.

Belzile, C., Guo, L., 2006. Optical properties of low molecular weight and colloidal organic matter: Application of the ultrafiltration permeation model to DOM absorption and fluorescence. Marine Chemistry 98 (2–4), 183–196.

Benner, R., Amon, R.M., 2015. The size-reactivity continuum of major bioelements in the ocean. Annu. Rev. Mar. Sci 7, 185–205.

Bianchi, et al., 2013. Enhanced transfer of terrestrially derived carbon to the atmosphere in a flooding event. Geophys. Res. Lett. 40, 116–122. https://doi.org/10.1029/2012GL054145.

Bianchi, T.S., Lambert, C.D., Santschi, P.H., Guo, L., 1997. Sources and transport of land-derived particulate and dissolved organic matter in the Gulf of Mexico (Texas shelf/slope): the use of ligninphenols and loliolides as biomarkers. Org. Geochem. 27, 65–78. https://doi.org/10.1016/s0146-6380(97)00040-5.

Bianchi, T.S., Pennock, J.R., Twilley, 1998. Biogeochemistry of Gulf of Mexico Estuaries, R.R. eds. John Wiley & Sons.

Bianchi, T.S., Filley, T., Dria, K., Hatcher, P.G., 2004. Temporal variability in sources of dissolved organic carbon in the lower Mississippi River. Geochim. Cosmochim. Acta 68, 959–967.

Broecker, W.S., Peng, T.H., 1982. Tracers in the Sea, vol. 690. Lamont-Doherty Geol. Obs., Columbia University, Palisades, New York.

Brogi, S.R., Balestra, C., Casotti, R., Cossarini, G., Galletti, Y., Gonnelli, M., Vestri, S., Santinelli, C., 2020. Time resolved data unveils the complex DOM dynamics in a Mediterranean river. Sci. Total Environ. 733, 139212.

Cai, Y., Guo, L., 2009. Abundance and variation of colloidal organic phosphorus in riverine, estuarine, and coastal waters in the northern Gulf of Mexico. Limnol. Oceanogr. 54 (4), 1393–1402. https://doi.org/10.4319/lo.2009.54.4.1393.

Cai, Y., Guo, L., Wang, X., Lohrenz, S.E., Mojzis, A.K., 2013. Effects of tropical cyclones on river chemistry: a case study of the lower Pearl River during hurricanes Gustav and Ike. Estuar. Coast. Shelf Sci. 129, 180–188.

Cai, Y., Guo, L., Wang, X., Aiken, G., 2015. Abundance, stable isotopic composition, and export fluxes of DOC, POC, and DIC from the lower Mississippi River during 2006–2008. J. Geophys. Res. Biogeosci. 120 (11), 2273–2288.

Cai, Y., Shim, M.J., Guo, L., Shiller, A., 2016. Floodplain influence on carbon speciation and fluxes from the lower Pearl River, Mississippi. Geochim. Cosmochim. Acta 186, 189–206.

Cai, Y., You, C.F., Wu, S.F., Cai, W.J., Guo, L., 2020. Seasonal variations in strontium and carbon isotope systematics in the lower Mississippi River: implications for chemical weathering. Chem. Geol. 553, 119810.

Chen, M., Jaffé, R., 2016. Quantitative assessment of photo-and bio-reactivity of chromophoric and fluorescent dissolved organic matter from biomass and soil leachates and from surface waters in a subtropical wetland. Biogeochemistry 129, 273–289.

Coble, P.G., 1996. Characterization of marine and terrestrial DOM in seawater using excitation-emission matrix spectroscopy. Mar. Chem. 51, 325–346. https://doi.org/10.1016/0304-4203(95)00062-3.

Coble, P.G., 2007. Marine optical biogeochemistry: the chemistry of ocean color. Chem. Rev. 107 (2), 402–418.

Coble, P.G., Del Castillo, Avril, B., 1998. Distribution and optical properties of CDOM in the Arabian Sea during the 1995 Southwest Monsoon. *Deep Sea Research Part II*. Topical Studies in Oceanography 45, 2195–2223.

Cory, R.M., Miller, M.P., McNight, D.M., Guerard, J.J., Miller, P.L., 2010. Effect of instrument-specific response on the analysis of fulvic acid fluorescence spectra. Limnol. Oceanogr. Methods 8, 67–78.

Cronan, C.S., Aiken, G.R., 1985. Chemistry and transport of soluble humic substances in forested watersheds of the Adirondack Park, New York. Geochim. Cosmochim. Acta 49 (8), 1697–1705. https://doi.org/10.1016/0016-7037(85)90140-1.

Dagg, M.J., et al., 2005. Biogeochemical characteristics of the lower Mississippi River, USA, during June 2003. Estuaries 28 (5), 664–674.

Dalzell, B.J., Filley, T.R., Harbor, J.M., 2005. Flood pulse influences on terrestrial organic matter export from an agricultural watershed. J. Geophys. Res. 110 (G2), G02011. https://doi.org/10.1029/2005jg000043.

DeVilbiss, S.E., Zhou, Z., Klump, J.V., Guo, L., 2016. Spatiotemporal variations in the abundance and composition of bulk and Chromophoric dissolved organic matter in seasonally hypoxia-influenced Green Bay, Lake Michigan, USA. Sci. Total Environ. 565, 742–757.

D'Sa, E.J., DiMarco, S.F., 2009. Seasonal variability and controls on chromophoric dissolved organic matter in a large river-dominated coastal margin. Limnol. Oceanogr. 54 (6), 2233–2242.

D'Sa, E.J., Overton, E.B., Lohrenz, S.E., Maiti, K., Turner, R.E., Freeman, A., 2016. Changing dynamics of dissolved organic matter fluorescence in the northern Gulf of Mexico following the Deepwater horizon oil spill. Environ. Sci. Technol. 50, 4940–4950.

D'Sa, E.J., Tzortziou, M., Liu, B., 2023. Extreme events and impacts on organic carbon cycles from ocean color remote sensing: review with case study, challenges, and future directions. Earth Sci. Rev. 243, 104503.

Duan, S., Bianchi, T.S., Sampere, T.P., 2007a. Temporal variability in the composition and abundance of terrestrially-derived dissolved organic matter in the lower Mississippi and pearl Rivers. Mar. Chem. 103, 172–184. https://doi.org/10.1016/j.marchem.2006.07.003.

Duan, S., et al., 2007b. Variability in the bulk composition and abundance of dissolved organic matter in the lower Mississippi and pearl rivers. J. Geophys. Res. 112 (G2), G02024. https://doi.org/10.1029/2006JG000206.

Duan, S., et al., 2013. Transport and biogeochemical cycles of organic carbon and nutrients in the lower Mississippi River. In: Bianchi, T.S., Allison, M.A., Cai, W.-J. (Eds.), Biogeochemical Dynamics at Major River-Coastal Interfaces: Linkages with Global Change. Cambridge University Press, New York, USA.

Duan, S., He, Y., Kaushal, S.S., Bianchi, T.S., Ward, N.D., Guo, L., 2017. Impact of wetland decline on decreasing dissolved organic carbon concentrations along the Mississippi River continuum. Front. Mar. Sci. 3, 280. https://doi.org/10.3389/fmars.2016.00280.

Engelhaupt, E., Bianchi, T.S., 2001. Sources and composition of high-molecular-weight dissolved organic carbon in a southern Louisiana tidal stream (bayou Trepagnier). Limnol. Oceanogr. 46 (4), 917–926.

Évrard, A., Fink-Mercier, C., Galindo, V., Neumeier, U., Gosselin, M., Xie, H., 2023. Regulated vs. unregulated rivers: impacts on CDOM dynamics in the eastern James Bay. Mar. Chem. 256, 104309.

Fichot, C.G., Benner, R., 2014. The fate of terrigenous dissolved organic carbon in a river-influenced ocean margin. Glob. Biogeochem. Cycles 28 (3), 300–318.

Findlay, S., Sinsabaugh, R.L., 1999. Unravelling the sources and bioavailability of dissolved organic matter in lotic aquatic ecosystems. Mar. Freshw. Res. 50 (8), 781–790. https://doi.org/10.1071/MF99069.

Findlay, S., Sinsabaugh, R.L., Fischer, D.T., Franchini, P., 1998. Sources of dissolved organic carbon supporting planktonic bacterial production in the tidal freshwater Hudson river. Ecosystems 1 (3), 227–239. https://doi.org/10.1007/s100219900018.

Goolsby, D.A., Battaglin, W.A., 2001. Long-term changes in concentrations and flux of nitrogen in the Mississippi River basin, USA. Hydrol. Process. 15 (7), 1209–1226. https://doi.org/10.1002/hyp.210.

Guéguen, C., Guo, L., Tanaka, N., 2005. Distributions and characteristics of colored dissolved organic matter in the Western Arctic Ocean. Cont. Shelf Res. 25 (10), 1195–1207.

Guéguen, C., Guo, L., Yamamoto-Kawai, M., Tanaka, N., 2007. Colored dissolved organic matter dynamics across the shelf-basin interface in the western Arctic Ocean. J. Geophys. Res. Oceans 112 (C5), C05038.

Guo, M., Chorover, J., 2003. Transport and fractionation of dissolved organic matter in soil columns. Soil Sci. 168 (2), 108–118.

Guo, L., Macdonald, R.W., 2006. Source and transport of terrigenous organic matter in the upper Yukon River: evidence from isotope ($\delta^{13}C$,$\Delta^{14}C$, and $\delta^{15}N$) composition of dissolved, colloidal, and particulate phases. Glob. Biogeochem. Cycles 20 (2). https://doi.org/10.1029/2005gb002593. GB2011.

Guo, L., Santschi, P.H., 1996. A critical evaluation of the cross-flow ultrafiltration technique for sampling colloidal organic carbon in seawater. Mar. Chem. 55, 113–127.

Guo, L, Santschi, PH, 1997. Measurements of dissolved organic carbon (DOC) in sea water by high temperature combustion method. Acta oceanologica sinica 16 (3), 339–353.

Guo, L., Santschi, P.H., 2007. Ultrafiltration and its applications to sampling and characterisation of aquatic colloids. In: Wilkinson, K.J., Lead, J.R. (Eds.), Environmental colloids and particles. John Wiley and Sons, Ltd, pp. 159–221. https://doi.org/10.1002/9780470024539.ch4.

Guo, L., Santschi, P.H., Warnken, K.W., 1995. Dynamics of dissolved organic carbon (DOC) in oceanic environments. Limnol. Oceanogr. 40 (8), 1392–1403.

Guo, L., Santschi, P.H., Cifuentes, L.A., Trumbore, S.E., Southon, J., 1996. Cycling of high-molecular-weight dissolved organic matter in the middle Atlantic bight as revealed by carbon isotopic (13C and 14C) signatures. Limnol. Oceanogr. 41 (6), 1242–1252. https://doi.org/10.4319/lo.1996.41.6.1242.

Guo, L., White, M., Xu, C., Santschi, P.H., 2009. Chemical and isotopic composition of high molecular weight dissolved organic matter from the Mississippi River plume. Mar. Chem. 114, 63–71.

Guo, L., Cai, Y., Belzile, C., Macdonald, R.W., 2012. Sources and export fluxes of inorganic and organic carbon and nutrient species from the seasonally ice-covered Yukon River. Biogeochemistry 107, 187–206.

Hanley, K.W., Wollheim, W.M., Salisbury, J., Huntington, T., Aiken, G., 2013. Controls on dissolved organic carbon quantity and chemical character in temperate rivers of North America. Glob. Biogeochem. Cycles 27 (2), 492–504.

Hedges, J.I., Keil, R.G., Benner, R., 1997. What happens to terrestrial organic matter in the ocean? Org. Geochem. 27 (5–6), 195–212. https://doi.org/10.1016/s0146-6380(97)00066-1.

Helms, J.R., et al., 2008. Absorption spectral slopes and slope ratios as indicators of molecular weight, source, and photobleaching of chromophoric dissolved organic matter. Limnol. Oceanogr. 53 (3), 955–969.
Hounshell, A.G., Rudolph, J.C., Van Dam, B.R., Hall, N.S., Osburn, C.L., Paerl, H.W., 2019. Extreme weather events modulate processing and export of dissolved organic carbon in the Neuse River estuary, NC. Estuar. Coast. Shelf Sci. 219, 189–200.
Huguet, A., et al., 2009. Properties of fluorescent dissolved organic matter in the Gironde estuary. Org. Geochem. 40 (6), 706–719. https://doi.org/10.1016/j.orggeochem.2009.03.002.
Jaffé, R., et al., 2008. Spatial and temporal variations in DOM composition in ecosystems: the importance of long-term monitoring of optical properties. J. Geophys. Res. 113 (G4), G04032. https://doi.org/10.1029/2008jg000683.
Joung, D., Guo, L., Shiller, A.M., 2019. Role of the Atchafalaya River basin in regulating export fluxes of dissolved organic carbon, nutrients, and trace elements to the Louisiana shelf. J. Hydrol. X 2, 100018. https://doi.org/10.1016/j.hydroa.2019.100018.
Kida, M., Taichi, K., Yukiko, T., Kentaro, H., Sakae, K., Nagamitsu, M., Nobuhide, F., 2019. Origin, distributions, and environmental significance of ubiquitous humic-like fluorophores in Antarctic lakes and streams. Water Res. 163, 114901.
Li, M., Peng, C., Wang, M., Xue, W., Zhang, K., Wang, K., Shi, G., Zhu, Q., 2017. The carbon flux of global rivers: a re-evaluation of amount and spatial patterns. Ecol. Indic. 80, 40–51.
Lin, H., Guo, L., 2020. Variations in colloidal DOM composition with molecular weight within individual water samples as characterized by flow field-flow fractionation and EEM-PARAFAC analysis. Environ. Sci. Technol. 54, 1657–1667. https://doi.org/10.1021/acs.est.9b07123.
Lin, H., Xu, H., Cai, Y., Belzile, C., Macdonald, R.W., Guo, L., 2021. Dynamic changes in size-fractionated dissolved organic matter composition in a seasonally ice-covered Arctic River. Limnol. Oceanogr. 66, 3085–3099. https://doi.org/10.1002/lno.11862.
Liao, C., Zhuang, Q., Leung, L.R., Guo, L., 2019. Quantifying dissolved organic carbon dynamics using a three-dimensional terrestrial ecosystem model at high spatial-temporal resolutions. Journal of Advances in Modeling Earth Systems 11, 4489–4512.
Lin, H., Bartlett, S.L., Guo, L., 2023. Distinct variations in fluorescent DOM components along a trophic gradient in the lower Fox River-Green Bay as characterized using one-sample PARAFAC approach. Sci. Total Environ. 902, 165891.
Liu, B., D'Sa, E.J., Joshi, I., 2019. Multi-decadal trends and influences on dissolved organic carbon distribution in the Barataria basin, Louisiana from in-situ and Landsat/ MODIS observations. Remote Sens. Environ. 228, 183–202.
Liu, B., D'Sa, E.J., Messina, F., Baustian, M.M., Maiti, K., Rivera-Monroy, V., Huang, W., Georgiou, I.Y., 2023. Dissolved organic carbon dynamics and fluxes in Mississippi-Atchafalaya deltaic system impacted by an extreme flood event and hurricanes: a multi-satellite approach using Sentinel-2/3 and Landsat-8/9 Data. Front. Mar. Sci. 10, 1159367.
Lu, K., Liu, Z., 2019. Molecular level analysis reveals changes in chemical composition of dissolved organic matter from South Texas Rivers after high flow events. Front. Mar. Sci. 6, 673. https://doi.org/10.3389/fmars.2019.00673.
Lu, Y., Bauer, J.E., Canuel, E.A., Yamashita, Y., Chambers, R.M., Jaffé, R., 2013. Photochemical and microbial alteration of dissolved organic matter in temperate headwater streams associated with different land use. J. Geophys. Res. Biogeosci. 118 (2), 566–580.
Lu, K., Xue, J., Guo, L., Liu, Z., 2023. The bio-and thermal lability of dissolved organic matter as revealed by high-resolution mass spectrometry and thermal chemical analyses. Mar. Chem. 250, 104184.
Malcolm, R.L., Durum, W.H., 1976. Organic carbon and nitrogen concentrations and annual organic carbon load of six selected rivers of the United States. In: Geological Survey Water-Supply Paper 1817-F, pp. 1–29.
Mattsson, T., Kortelainen, P., Raike, A., 2005. Export of DOM from boreal catchments: impacts of land use cover and climate. Biogeochemistry 76 (2), 373–394.
McKnight, D.M., et al., 2001. Spectrofluorometric characterization of dissolved organic matter for indication of precursor organic material and aromaticity. Limnol. Oceanogr. 46 (1), 38–48.
Meade, R.H., Yuzyk, T.R., Day, T.J., 1990. Movement and storage of sediment in rivers of the United States and Canada. In: Wolman, M.G., Riggs, H.C. (Eds.), Surface Water Hydrology. Geological Society of America, Boulder, Colorado, pp. 255–280.
Milliman, J., 1992. Flux and fate of fluvial sediment and water in coastal seas. In: Mantoura, R., Martin, J.M., Wollast, R. (Eds.), Ocean Margin Processes in Global Change. John Wiley & Sons, New York.
Murphy, K.R., Butler, K.D., Spencer, R.G.M., Stedmon, C.A., Boehme, J.R., Aiken, G.R., 2010. Measurement of dissolved organic matter fluorescence in aquatic environments: an interlaboratory comparison. Environ. Sci. Technol. 44, 9405–9412.
Murphy, K.R., Stedmon, C.A., Graeber, D., Bro, R., 2013. Fluorescence spectroscopy and multi-way techniques. PARAFAC. Analyt. Meth. 5 (23), 6557–6566. https://doi.org/10.1039/c3ay41160e.
Murphy, K.R., Timko, S.A., Gonsior, M., Powers, L.C., Wunsch, U.J., Stedmon, C.A., 2018. Photochemistry illuminates ubiquitous organic matter fluorescence spectra. Environ. Sci. Technol. 52, 11243–11250.
Nugyen, H.V., Hur, J., Shin, H.S., 2010. Changes in spectroscopic and molecular weight characteristics of dissolved organic matter in a river during a storm event. Water Air Soil Pollut. 212 (1–4), 395–406.
Osburn, C., Morris, D., Thorn, K., Moeller, R., 2001. Chemical and optical changes in freshwater dissolved organic matter exposed to solar radiation. Biogeochemistry 54 (3), 251–278. https://doi.org/10.1023/a:1010657428418.
Raymond, P.A., Spencer, R.G.M., 2015. Riverine DOM. In: Hansell, D.A., Carlson, C.A. (Eds.), Biogeochemistry of Marine Dissolved Organic Matter, Second edn. Academic Press, Boston, MA, pp. 509–533. https://doi.org/10.1016/b978-0-12-405940-5.00011-x.ESL.
Shen, Y., Fichot, C.G., Benner, R., 2012. Floodplain influence on dissolved organic matter composition and export from the Mississippi-Atchafalaya River system to the Gulf of Mexico. Limnol. Oceanogr. 57 (4), 1149–1160.
Spencer, R.G.M., Butler, K.D., Aiken, G.R., 2012. Dissolved organic carbon and Chromophoric dissolved organic matter properties of Rivers in the USA. J. Geophys. Res. Biogeosci. 117 (G3).
Stackpoole, S.M., Stets, E.G., Clow, D.W., Burns, D.A., Aiken, G.R., Aulenbach, B.T., Creed, I.F., Hirsch, R.M., Laudon, H., Pellerin, B.A., Striegl, R.G., 2017. Spatial and temporal patterns of dissolved organic matter quantity and quality in the Mississippi River basin, 1997–2013. Hydrol. Process. 31 (4), 902–915.
Stedmon, C.A., Bro, R., 2008. Characterizing dissolved organic matter fluorescence with parallel factor analysis: a tutorial. Limnol. Oceanogr. Methods 6, 572–579. https://doi.org/10.4319/lom.2008.6.572.
Stedmon, C.A., Markager, S., Bro, R., 2003. Tracing dissolved organic matter in aquatic environments using a new approach to fluorescence spectroscopy. Mar. Chem. 82(, 239–254. https://doi.org/10.1016/s0304-4203(03)00072-0.
Stolpe, B., Guo, L., Shiller, A.M., Hassellöv, M., 2010. Size and composition of colloidal organic matter and trace elements in the Mississippi River, Pearl River and the northern Gulf of Mexico, as characterized by flow field-flow fractionation. Mar. Chem. 118, 119–128.
Stolpe, B., Zhou, Z., Guo, L., Shiller, A.M., 2014. Colloidal size distribution of humic-and protein-like fluorescent organic matter in the northern Gulf of Mexico. Mar. Chem. 164, 25–37.
Tehrani, N.C., D'Sa, E.J., Osburn, C.L., Bianchi, T.S., Schaeffer, B.A., 2013. Chromophoric dissolved organic matter and dissolved organic carbon from sea-viewing wide field-of-view sensor (SeaWiFS), moderate resolution imaging spectroradiometer (MODIS) and MERIS sensors: case study for the northern gulf of Mexico. Remote Sens. 5, 1439–1464.
Ward, N.D., Bianchi, T.S., Medeiros, P.M., Seidel, M., Richey, J.E., Keil, R.G., et al., 2017. Where carbon goes when water flows: carbon cycling across the aquatic continuum. Front. Mar. Sci. 4 https://doi.org/10.3389/fmars.2017.00007.
Warnken, K.W., Santschi, P.H., 2004. Biogeochemical behavior of organic carbon in the Trinity River downstream of a large reservoir lake in Texas, USA. Sci. Total Environ. 329, 131–144.
Weishaar, J.L., et al., 2003. Evaluation of specific ultraviolet absorbance as an indicator of the chemical composition and reactivity of dissolved organic carbon. Environ. Sci. Technol. 37 (20), 4702–4708. https://doi.org/10.1021/es030360x.
Wünsch, U.J., Murphy, K.R., Stedmon, C.A., 2017. The one-sample PARAFAC approach reveals molecular size distributions of fluorescent components in dissolved organic matter. Environ. Sci. Technol. 51 (20), 11900–11908.
Wünsch, U.J., Bro, R., Stedmon, C.A., Wenig, P., Murphy, K., 2019. Emerging patterns in the global distribution of dissolved organic matter fluorescence. Anal. Method. 11, 888–893.
Xu, H., Guo, L., 2017. Molecular size-dependent abundance and composition of dissolved organic matter in river, Lake and Sea Waters. Water Res. 117, 115–126.
Xu, H., Houghton, E.M., Houghton, C.J., Guo, L., 2018. Variations in size and composition of colloidal organic matter in a negative freshwater estuary. Sci. Total Environ. 615, 931–941.
Yano, Y., Lajtha, K., Sollins, P., Caldwell, B.A., 2005a. Chemical and seasonal controls on the dynamics of dissolved organic matter in a coniferous old-growth stand in the Pacific northwest, USA. Biogeochemistry 71 (2), 197–223. https://doi.org/10.1007/s10533-004-8130-8.
Yano, Y., Lajtha, K., Sollins, P., Caldwell, B.A., 2005b. Chemistry and dynamics of dissolved organic matter in a temperate coniferous forest on andic soils: effects of litter quality. Ecosystems 8 (3), 286–300. https://doi.org/10.1007/s10021-005-0022-9.
Zhao, L., Gao, L., Guo, L., 2021. Seasonal variations in molecular size of chromophoric dissolved organic matter from the lower Changjiang (Yangtze) River. J. Geophys. Res. Biogeosci. 126 (8) e2020JG006160.
Zhou, Z., Guo, L., 2012. Evolution of the optical properties of seawater influenced by the Deepwater horizon oil spill in the Gulf of Mexico. Environ. Res. Lett. 7 (2), 025301 https://doi.org/10.1088/1748-9326/7/2/025301.
Zhou, Z., Guo, L., Shiller, A.M., Lohrenz, S.E., Asper, V.L., Osburn, C.L., 2013. Characterization of oil components from the Deepwater horizon oil spill in the Gulf of Mexico using fluorescence EEM techniques. Mar. Chem. 148, 10–21. https://doi.org/10.1016/j.marchem.2012.10.003.
Zhou, Z., Guo, L., Minor, E.C., 2016a. Characterization of bulk and chromophoric dissolved organic matter in the Laurentian Great Lakes. J. Great Lakes Res. 42, 789–801.
Zhou, Z., Stolpe, B., Guo, L., Shiller, A.M., 2016b. Colloidal size spectra, composition and estuarine mixing behavior of DOM in river and estuarine waters of the northern Gulf of Mexico. Geochim. Cosmochim. Acta 181, 1–17.
Zou, L., Sun, M.Y., Guo, L., 2006. Temporal variations of organic carbon inputs into the upper Yukon River: Evidence from fatty acids and their stable carbon isotopic compositions in dissolved, colloidal and particulate phases. Organic Geochemistry 37 (8), 944–956.
Zsolnay, A., Baigar, E., Jimenez, M., Steinweg, B., Saccomandi, F., 1999. Differentiating with fluorescence spectroscopy the sources of dissolved organic matter in soils subjected to drying. Chemosphere 38, 45–50.